The heat flux of horizontal convection: definition of the Nusselt number

Cesar B. Rocha[1]†, Navid C. Constantinou[2], Stefan G. Llewellyn Smith[3], and William R. Young[4]

[1]Department of Physical Oceanography, Woods Hole Oceanographic Institution, Woods Hole, MA 02543, USA

[2]Research School of Earth Sciences and ARC Centre of Excellence for Climate Extremes, Australian National University, ACT 2601, Australia

[3]Department of Mechanical and Aerospace Engineering, University of California San Diego, 9500 Gilman Drive, La Jolla, CA 92093-0411, USA

[4]Scripps Institution of Oceanography, University of California San Diego, 9500 Gilman Drive, La Jolla, CA 92093-0213, USA

(Received xx; revised xx; accepted xx)

We consider the problem of horizontal convection in which non-uniform buoyancy, $b_s(x, y)$, is imposed on the top surface of a container and all other surfaces are insulating. Horizontal convection produces a net horizontal flux of buoyancy, $\boldsymbol{J}$, defined by vertically and temporally averaging the interior horizontal flux of buoyancy. We show that $\overline{\boldsymbol{J} \cdot \boldsymbol{\nabla} b_s} = -\kappa \langle |\boldsymbol{\nabla} b|^2 \rangle$; the overbar denotes a space-time average over the top surface, angle brackets denote a volume-time average and κ is the molecular diffusivity of buoyancy b. This connection between $\boldsymbol{J}$ and $\kappa \langle |\boldsymbol{\nabla} b|^2 \rangle$ justifies the definition of the horizontal-convective Nusselt number, Nu, as the ratio of $\kappa \langle |\boldsymbol{\nabla} b|^2 \rangle$ to the corresponding quantity produced by molecular diffusion alone. We discuss the advantages of this definition of Nu over other definitions of horizontal-convective Nusselt number currently in use. We investigate transient effects and show that $\kappa \langle |\boldsymbol{\nabla} b|^2 \rangle$ equilibrates more rapidly than other global averages, such as the domain averaged kinetic energy and bottom buoyancy.

1. Introduction

Horizontal convection (HC) is convection generated in a fluid layer $0 < z < h$ by imposing non-uniform buoyancy along the top surface $z = h$; all other bounding surfaces are insulated (Rossby 1965; Hughes & Griffiths 2008). HC is a basic problem in fluid mechanics and serves as an interesting counterpoint to the much more widely studied problem of Rayleigh-Bénard convection (RBC) in which the fluid layer is heated at the bottom, $z = 0$ and cooled the top, $z = h$.

In RBC the correct definition of the Nusselt number, Nu, is clear: after averaging over (x, y, t) there is a constant vertical heat flux passing through every level of constant z between 0 and h. By definition, the RBC Nu is the constant vertical heat flux through the layer divided by the diffusive heat flux of the unstable static solution.

In HC, however, there is zero net vertical heat flux through every level of constant z, e.g., see (2.6) below. Thus the RBC definition of Nu is not applicable to HC. Indeed, one expects that in HC the Nusselt number should have something to do with the *horizontal* flux of heat, $J(x)$ defined in (3.1) below. But there is no agreement on how to characterize the non-dimensional amplitude of the function $J(x)$ with a single number. For example,

† Email address for correspondence: crocha@whoi.edu

some authors define a Nusselt number by normalizing

$$\max_{\forall x} J(x) \tag{1.1}$$

with the corresponding maximum of the conductive heat flux. There are, however, three or four other definitions of Nu current in the HC literature (discussed further in section 3). This discord complicates quantitative comparison between the results of different authors. Moreover it is disturbing that the most basic index of the strength of HC seems to be a matter of opinion.

This paper shows that the HC Nusselt number is best defined as

$$Nu \stackrel{\text{def}}{=} \frac{\chi}{\chi_{\text{diff}}}\,. \tag{1.2}$$

In definition (1.2), χ is the dissipation of buoyancy (or thermal) variance defined in (3.5) below and χ_{diff} is the corresponding quantity of the diffusive (i.e., zero Rayleigh number) solution. The ratio on the right of (1.2) was introduced as a non-dimensional index of the strength of HC by Paparella & Young (2002). But because there seemed to be no clear connection to the horizontal heat flux, $J(x)$, Paparella & Young (2002) did not refer to χ/χ_{diff} as a "Nusselt number". Although χ/χ_{diff} has been used as an index of HC in a few subsequent papers (Siggers *et al.* 2004; Scotti & White 2011), most authors prefer to define a HC Nusselt number with a more obvious connection to the horizontal heat flux $J(x)$ in (3.1). In section 3 we address this concern by establishing a relation between the χ-based Nu in (1.2) and the horizontal heat flux $J(x)$. This justifies referring to χ/χ_{diff} as a Nusselt number and we note other advantages that strongly compel (1.2) as the best definition of a horizontal-convective Nu.

In section 2 we formulate the problem of horizontal convection. In section 3 we show that the horizontal-convective Nusselt number is best defined by (1.2). Section 4 discusses the transient adjustment of Nu in (1.2) to its long-time average. Section 5 is the conclusion.

2. Formulation of the horizontal convection problem

Consider a Boussinesq fluid with density $\rho = \rho_0(1 - g^{-1}b)$, where ρ_0 is a constant reference density, b is the "buoyancy," and g is the gravitational acceleration. If the fluid is stratified by temperature variations then $b = g\alpha(T - T_0)$, where T_0 is a reference temperature and α is the thermal expansion coefficient. The Boussinesq equations of motion are

$$\boldsymbol{u}_t + \boldsymbol{u}\cdot\boldsymbol{\nabla}\boldsymbol{u} + \boldsymbol{\nabla}p = b\hat{\boldsymbol{z}} + \nu\triangle\boldsymbol{u}\,, \tag{2.1}$$

$$b_t + \boldsymbol{u}\cdot\boldsymbol{\nabla}b = \kappa\triangle b\,, \tag{2.2}$$

$$\boldsymbol{\nabla}\cdot\boldsymbol{u} = 0\,. \tag{2.3}$$

The kinematic viscosity is ν, the thermal diffusivity is κ and $\triangle = \partial_x^2 + \partial_y^2 + \partial_z^2$ is the Laplacian.

2.1. *Horizontal convective boundary conditions and control parameters*

We suppose the fluid occupies a rectangular domain with depth h, length ℓ_x, width ℓ_y; we assume periodicity in the horizontal directions, x and y. At the bottom surface ($z = 0$) and top surface ($z = h$) the boundary conditions on the velocity $\boldsymbol{u} = (u, v, w)$ are $w = 0$ and for the viscous boundary condition either no slip, $u = v = 0$, or free slip, $u_z = v_z = 0$. At $z = 0$ the buoyancy boundary condition is no flux, $\kappa b_z = 0$ and at the top, $z = h$,

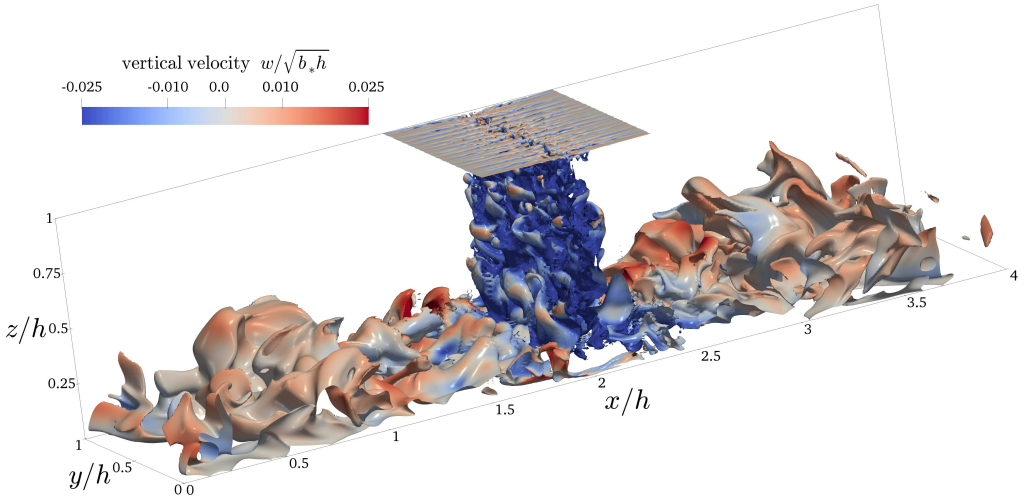

FIGURE 1. A snapshot of the $b = -0.7964 b_\star$ surface at $\kappa t/h^2 = 0.12$ for a 3D horizontal-convective flow; colors denote the vertical velocity. This is a no-slip solution with sinusoidal surface buoyancy b_s in (2.4); control parameters are $Ra = 6.4 \times 10^{10}$, $Pr = 1$, $A_x = 4$ and $A_y = 1$.

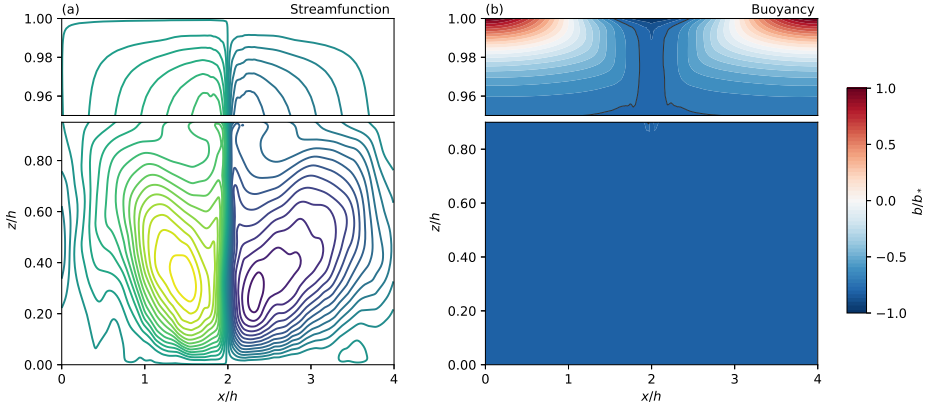

FIGURE 2. Snapshots of (a) streamfunction, calculated from the y-averaged velocity (u, w), and (b) the y-averaged buoyancy at $\kappa t/h^2 = 0.12$. This is the same solution as that of figure 1. The streamfunction in panel (a) is defined by the y-average of u and w. The black contour in panel (b) is $b = -0.79 b_\star$, which is close to the bottom buoyancy, defined as the (x, y, t)-average of b at $z = 0$.

the boundary condition is $b = b_\mathrm{s}(x)$, where the top surface buoyancy b_s is a prescribed function of x. As a surface buoyancy field we use

$$b_\mathrm{s}(x) = b_\star \cos(2\pi x/\ell_x)\,. \tag{2.4}$$

Figure 1 shows a 3D HC flow with no-slip boundary conditions and the surface buoyancy (2.4). Figure 2 shows y-averaged buoyancy and the overturning streamfunction calculated by the y-averaging the 3D velocity. These figures illustrate three main large-scale features of HC: a buoyancy boundary layer pressed against the non-uniform upper surface and uniform buoyancy in the deep bulk; an entraining plume beneath the densest point on the upper surface; and interior upwelling towards the nonuniform surface in the bulk of the domain.

The problem is characterized by four non-dimensional parameters: the Rayleigh and Prandtl numbers

$$Ra \stackrel{\text{def}}{=} \frac{\ell_x^3 b_\star}{\nu\kappa}\,, \qquad \text{and} \qquad Pr \stackrel{\text{def}}{=} \frac{\nu}{\kappa}\,, \tag{2.5}$$

and the aspect ratios $A_x \stackrel{\text{def}}{=} \ell_x/h$ and $A_y \stackrel{\text{def}}{=} \ell_y/h$. Two-dimensional HC corresponds to $A_y = 0$.

2.2. *Horizontal-convective power integrals*

We use an overbar to denote an average over x, y and t, taken at any fixed z and angle brackets to denote a total volume average over x, y, z and t. Using this notation, we recall some results from Paparella & Young (2002) that are used below.

Horizontally averaging the buoyancy equation (2.2) we obtain the zero-flux constraint

$$\overline{wb} - \kappa \bar{b}_z = 0\,. \tag{2.6}$$

Forming $\langle \boldsymbol{u}\cdot(2.1)\rangle$, we obtain the kinetic energy power integral

$$\varepsilon = \langle wb\rangle\,, \tag{2.7}$$

where $\varepsilon \stackrel{\text{def}}{=} \nu\langle|\boldsymbol{\nabla u}|^2\rangle$ is the rate of dissipation of kinetic energy and $\langle wb\rangle$ is rate of conversion between potential and kinetic energy.

Vertically integrating (2.6) from $z = 0$ to h, and assuming that $\overline{b_{\rm s}} = 0$, we obtain another expression for $\langle wb\rangle$; substituting this into (2.7) we find

$$h\varepsilon = -\kappa\,\bar{b}(z=0)\,, \tag{2.8}$$

$$\leqslant \kappa\, b_\star\,. \tag{2.9}$$

In (2.8), $\bar{b}(z = 0)$ is the (x, y, t)-average of the buoyancy at the bottom $z = 0$. The inequality (2.9) follows from the extremum principle for the buoyancy advection-diffusion equation (2.2) with boundary condition (2.4). In the example shown in figure 1 the bottom buoyancy is $\bar{b}(z = 0) \approx -0.83 b_\star$ and thus the right of inequality (2.9) is about 20% larger than ε.

3. Definition of the horizontal-convective Nusselt number

For equilibrated HC the vertical buoyancy flux is zero through every level — see (2.6) — and cannot be used to define an RB-type Nusselt number. Moreover, with specified $b_{\rm s}(x)$, buoyancy is transported along the x-axis and it is natural to consider the net horizontal flux,

$$J(x) \stackrel{\text{def}}{=} \text{tavg}\left[\frac{1}{h\ell_y}\int_0^{\ell_y}\!\!\int_0^h (ub - \kappa b_x)\,\mathrm{d}z\mathrm{d}y\right]\,, \tag{3.1}$$

in defining an HC Nusselt number. Above, tavg indicates a time average used to remove unsteady fluctuations remaining after the average over the (y, z)-plane. But $J(x)$ is not constant and it is not initially obvious how to best define a single number out of $J(x)$ as an index of HC buoyancy transport.

Another measure of HC transport is provided by the averaged buoyancy flux through the non-uniformly heated surface at $z = h$:

$$F(x) \stackrel{\text{def}}{=} \text{tavg}\left[\frac{1}{\ell_y}\int_0^{\ell_y} \kappa b_z(x, y, h, t)\,\mathrm{d}y\right]\,. \tag{3.2}$$

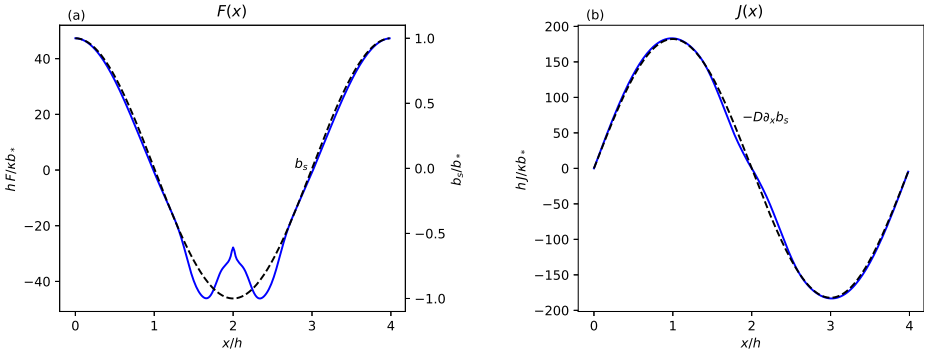

FIGURE 3. Left panel (a): the dashed black curve is the sinusoidal surface buoyancy profile in (2.4) and the solid blue curve is the vertical flux $F(x)$ defined in (3.2). Right panel (b) shows the horizontal flux $J(x)$ defined in (3.1) (the solid blue curve) and the relation (3.13) with D diagnosed from (3.16) (the dashed black curve). This is the same solution as that of figures 1 and 2.

Averaging the buoyancy equation (2.2) over the (y, z)-plane, and also over time, one finds that the divergence of the x-flux in (3.1) is equal to the flux in and out through the top:

$$h\frac{\mathrm{d}J}{\mathrm{d}x} = F\,. \tag{3.3}$$

Figure 3 exhibits the functions $J(x)$ and $F(x)$ for the $Ra = 6.4 \times 10^{10}$ solution shown in figure 1.

To obtain a single number as a measure of horizontal heat flux some authors define Nu using a normalized version of (1.1). Other authors define Nu based on the net buoyancy flux through that part of the non-uniformly heated surface with a destabilizing vertical buoyancy flux i.e., integrate $F(x)$ only over the region where $F(x) < 0$. Still others average $|F(x)|$ over x (which is greater by a factor of two than integration over the region with $F(x) < 0$). Yet another possibility is to integrate $F(x)$ over half of the boundary, that is over $0 < x < \ell_x/2$. These arbitrary definitions complicate quantitative comparison between Nusselt numbers reported in different papers.

Siggers *et al.* (2004) considered, and rejected, the Nusselt numbers discussed above as too difficult for theoretical work. The problem is that one does not know in advance where buoyancy flows into and out of the domain and it is difficult to get an analytic grip on $|F|$ or on $\max(J)$, still less on the flux through half of the boundary. As an indication of the difficulty, there is no proof that the various Nusselt numbers defined in the previous paragraph are greater than one. Indeed, some authors report Nusselt numbers less than one.

These issues are, to some extent, addressed by using piecewise constant surface forcing profiles (Mullarney *et al.* 2004; Gayen *et al.* 2013, 2014; Shishkina *et al.* 2016; Passaggia *et al.* 2017), such as

$$b_{\mathrm{s}}(x) = \begin{cases} +b_\star\,, & \text{for } -\ell_x/2 < x < 0\,; \\ -b_\star\,, & \text{for } 0 < x < +\ell_x/2\,. \end{cases} \tag{3.4}$$

The advantage of (3.4) is that the horizontal buoyancy flux through the discontinuity in $b_{\mathrm{s}}(x)$ — that is $J(0)$ — is distinguished and provides a "natural" definition of the horizontal-convective Nusselt number. It is unsatisfactory, however, to tie the definition of Nusselt number to a particular surface buoyancy condition $b_{\mathrm{s}}(x)$.

The alternative to (1.1) and similar constructions is to use the diffusive dissipation of

buoyancy variance,

$$\chi \stackrel{\text{def}}{=} \kappa\langle|\boldsymbol{\nabla} b|^2\rangle\,, \tag{3.5}$$

and define the Nusselt number as

$$Nu \stackrel{\text{def}}{=} \frac{\chi}{\chi_{\text{diff}}}\,, \tag{3.6}$$

where $\chi_{\text{diff}} \stackrel{\text{def}}{=} \kappa\langle|\boldsymbol{\nabla} b_{\text{diff}}|^2\rangle$ is the buoyancy dissipation of the diffusive solution i.e., $\kappa\triangle b_{\text{diff}} = 0$ with b_{diff} satisfying the same boundary conditions as b (Paparella & Young 2002; Siggers *et al.* 2004; Winters & Young 2009; Scotti & White 2011). It is straightforward to show that Nu in (3.6) is greater than unity.

Now χ in (3.5) does not have an obvious connection to the horizontal flux $J(x)$ in (3.1). This is probably why Nu in (3.6) has not been popular as an index of the strength of HC. For example, Siggers *et al.* (2004) refer to χ as a "pseudo-flux" because χ seems not to have a clear connection to the horizontal flux $J(x)$. But in (3.8) below we establish an integral relation between χ and J: this supports (3.6) as a useful definition of Nu.

Forming $\langle b\ (2.2)\rangle$ we obtain an identity expressing χ entirely in terms of conditions at the nonuniform surface $z = h$:

$$h\chi = \overline{Fb_{\text{s}}}\,, \tag{3.7}$$

where $F(x)$ is the vertical buoyancy flux in (3.2) and $b_{\text{s}}(x)$ is the nonuniform surface buoyancy. Using (3.3) to replace F in (3.7) by $\mathrm{d}J/\mathrm{d}x$, and integrating by parts in x, one finds

$$\overline{J\frac{\mathrm{d}b_{\text{s}}}{\mathrm{d}x}} = -\chi\,. \tag{3.8}$$

Thus χ is directly related to an x-average of $J(x)$, weighted by the surface buoyancy gradient: in this sense χ is a bulk index of the horizontal buoyancy flux. With (3.8) we see that the Nusselt number in (3.6) is equivalent to

$$Nu = \overline{J\frac{\mathrm{d}b_{\text{s}}}{\mathrm{d}x}} \Bigg/ \overline{J_{\text{diff}}\frac{\mathrm{d}b_{\text{s}}}{\mathrm{d}x}}\,, \tag{3.9}$$

where $J_{\text{diff}}(x)$ is the horizontal flux of the diffusive solution b_{diff}.

With the discontinuous $b_{\text{s}}(x)$ in (3.4), the surface buoyancy gradient is $2b_\star\delta(x)$ and (3.8) is particularly simple:

$$2b_\star J(0) = -\ell_x\chi\,. \tag{3.10}$$

In this case there is a direct connection between χ and the flux through the location of the discontinuous jump in buoyancy, i.e., the definition of Nu in (3.6) recovers the natural definition of Nusselt number associated with the discontinuous b_{s} in (3.4).

Nu in (3.6) has the advantage that it can also be applied to smoothly varying $b_{\text{s}}(x)$ such as the sinusoid in (2.4), or to the case with constant $\mathrm{d}b_{\text{s}}/\mathrm{d}x$ (Rossby 1965; Sheard & King 2011). Moreover, Nu in (3.6) copes with two-dimensional surface buoyancy distributions, $b_{\text{s}}(x, y)$, such as the examples recently considered by Rosevear *et al.* (2017). In this case, and in analogy with (3.1), one can define a two-dimensional buoyancy flux, $\boldsymbol{J}$, as the (z, t) average of $(ub - \kappa b_x)\hat{\boldsymbol{x}} + (vb - \kappa b_y)\hat{\boldsymbol{y}}$. Then it is easy to show that the generalizations of (3.3) and (3.8) are

$$h\boldsymbol{\nabla}\boldsymbol{\cdot}\boldsymbol{J} = F\,, \tag{3.11}$$

and

$$\overline{\boldsymbol{J}\boldsymbol{\cdot}\boldsymbol{\nabla} b_{\text{s}}} = -\chi\,. \tag{3.12}$$

Thus the horizontal buoyancy flux $\boldsymbol{J}$ is, on average, down the applied surface buoyancy gradient $\boldsymbol{\nabla} b_{\rm s}$, and χ emerges as a measure of this horizontal-convective transport.

The down-gradient direction of $\boldsymbol{J}$ suggests a relation between $\boldsymbol{J}$ and $\boldsymbol{\nabla} b_{\rm s}$ in terms of an "effective diffusivity", D. Thus we propose that

$$\boldsymbol{J} \approx -D \boldsymbol{\nabla} b_{\rm s} \,, \tag{3.13}$$

where D is a constant. An estimate of D is obtained by minimizing the squared error

$$E(D) \stackrel{\rm def}{=} \overline{|\boldsymbol{J} + D \boldsymbol{\nabla} b_{\rm s}|^2} \,. \tag{3.14}$$

Above, the overline denotes an (x, y) average. Setting $\mathrm{d}E/\mathrm{d}D$ to zero we obtain

$$D \stackrel{\rm def}{=} -\overline{\boldsymbol{J} \cdot \boldsymbol{\nabla} b_{\rm s}} \Big/ \overline{|\boldsymbol{\nabla} b_{\rm s}|^2} \,. \tag{3.15}$$

Substituting (3.12) into (3.15), the effective diffusivity, defined via minimization of $E(D)$, is diagnosed as

$$D = \kappa \left\langle |\boldsymbol{\nabla} b|^2 \right\rangle \Big/ \overline{|\boldsymbol{\nabla} b_{\rm s}|^2} \,. \tag{3.16}$$

In (3.16) the ratio $\left\langle |\boldsymbol{\nabla} b|^2 \right\rangle / \overline{|\boldsymbol{\nabla} b_{\rm s}|^2}$ emerges as an enhancement factor multiplying the molecular diffusivity κ to produce the effective diffusivity. Figure 3(b) compares the effective-diffusive flux in (3.13) against $J(x)$ for the solution shown in figures 1 and 2.

The Rayleigh-Bénard Nusselt number can also be expressed in the form (3.6) (Howard 1963; Doering & Constantin 1996). Thus the χ-based Nusselt number in (3.6) has the ancillary advantage of coinciding with that of Rayleigh-Bénard and focussing attention on χ as the fundamental quantity determining both the strength of transport and the vigor of mixing in all varieties of convection. Finally, χ is accessible to analysis so that variational methods can be used to establish bounds on the buoyancy transport of horizontal convection (Siggers *et al.* 2004; Winters & Young 2009; Rocha *et al.* 2020).

4. Equilibration of the Nusselt number

In this section we summarize the results of a numerical study directed at characterizing the transient adjustment of Nusselt number Nu in (3.6) to its long-time average. Thus in this section $Nu(t)$ is the "instantaneous Nusselt number" in which $\chi(t)$ is defined via a volume average (with no time averaging). We limit attention to $Pr = 1$ and the sinusoidal $b_{\rm s}(x)$ in (2.4) and discuss both no-slip and free-slip boundary conditions. We consider two-dimensional (2D) solutions with aspect ratios

$$\ell_x/h = 4 \,, \qquad \ell_y/h = 0 \,, \tag{4.1}$$

and three-dimensional (3D) solutions with

$$\ell_x/h = 4 \,, \qquad \ell_y/h = 1 \,. \tag{4.2}$$

We focus on $Ra = 6.4 \times 10^{10}$ — the same Ra used in figures 1 through 3. We find no important differences in the equilibration of Nu between these four cases (no slip versus free slip and 2D versus 3D).

These computations were performed with tools developed by the dedalus project: a spectral framework for solving partial differential equations (Burns *et al.* 2019, `www.dedalus-project.org`). We use Fourier bases in the horizontal, periodic directions and a Chebyshev basis in the vertical, and time-march the spectral equations using a fourth-order implicit-explicit Runge-Kutta scheme. For the 2D solutions the resolution

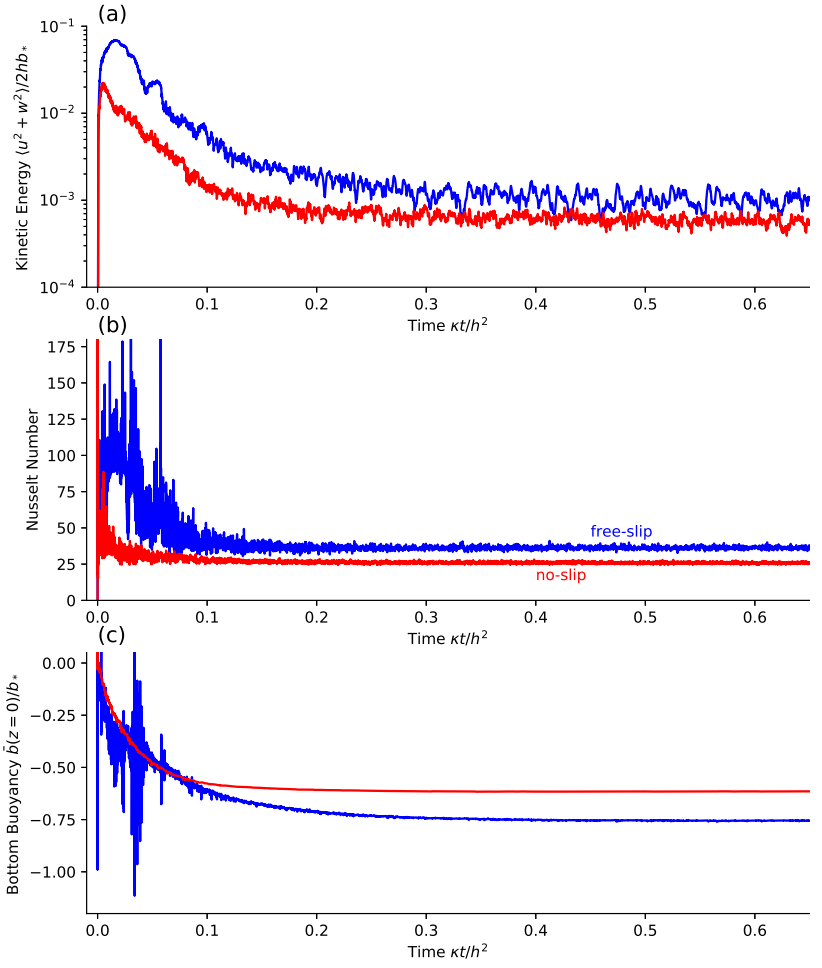

FIGURE 4. Approach to statistical equilibrium of two cases, one with the no-slip boundary condition (red curves) and the other with free slip (blue curves). Parameters are $Ra = 6.4\times10^{10}$, $Pr = 1$, $A_x = 4$ and $A_y = 0$ (two-dimensional solutions). The initial condition is $\boldsymbol{u} = 0$ and $b = 0$. (a) Domain-averaged kinetic energy, scaled with $b_\star h$. (b) The "instantaneous Nusselt number", $\chi/\chi_{\rm diff}$, with no time-averaging applied to χ. (c) The bottom buoyancy $\bar{b}(z=0)/b_\star$.

is $n_x \times n_z = 512 \times 128$, and for 3D $n_x \times n_y \times n_z = 512 \times 128 \times 128$. We tested the sensitivity of our results by halving this resolution and found only small differences.

Figure 4 shows the temporal evolution of the volume averaged kinetic energy, the Nusselt number (3.6) and the bottom buoyancy $\bar{b}(z=0)$ of two $Ra = 6.4\times10^{10}$ solutions: one with no-slip and the other with free-slip boundary conditions. Both solutions in figure 4 are two-dimensional ($A_y = 0$). The initial condition is $\boldsymbol{u} = b = 0$, i.e., the initial buoyancy is equal to the average of $b_{\rm s}(x)$ in (2.4). The bottom buoyancy in figure 4(c) appears as the energy source in (2.8) and in this sense the free-slip solution, with a larger value of $|\bar{b}(z=0)|$, is more strongly forced than the no-slip solution. By all three indices the free-slip flow has a stronger circulation than no-slip.

Both solutions in figure 4 slowly settle into a statistically steady state with persistent eddying time dependence associated with undulations of the plume that falls from beneath the densest point on the top surface, $z = h$. As noted by Wang & Huang (2005) and Ilicak & Vallis (2012), there is an active initial transient during which the flow is much

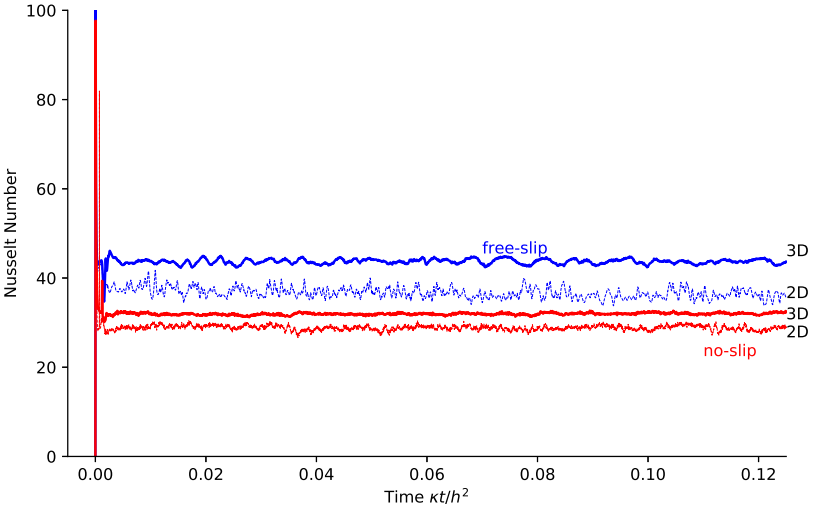

FIGURE 5. Rapid statistical equilibration of the Nusselt number of four $Ra = 6.4 \times 10^{10}$ solutions with the "cold-start" initial condition $b(\boldsymbol{x}, t = 0) = -0.74 b_*$.

more energetic than its long-time state, which is achieved on the diffusive timescale h^2/κ. The volume averaged kinetic energy in figure 4(a) transiently achieves values more than thirty times larger than the final value at the end of the computation $t = 0.65h^2/\kappa$. But most of this initial excitement subsides by about $t = 0.1h^2/\kappa$ and subsequently there is a slow transient adjustment lasting till the end of the computation. The kinetic energy and the bottom buoyancy are still slowly decreasing at $t = 0.65h^2/\kappa$. Fortunately, however, the Nusselt number in figure 4(b) reaches its final value significantly more rapidly than the other two indices, e.g., beyond about $t = 0.15h^2/\kappa$, $Nu(t)$ is stable. Probably this is because $Nu(t)$ is determined mainly by transport and mixing in the surface boundary layer, where $|\boldsymbol{\nabla} b|$ is largest. This shallow zone comes rapidly into statistical equilibrium. We conclude that the time average of $Nu(t)$ can be obtained with computations that are significantly shorter than the vertical diffusion time h^2/κ.

Griffiths *et al.* (2013) and Rossby (1998) have previously noted that adjustment of the boundary layer to perturbations in the surface buoyancy is very much faster than the diffusively-controlled adjustment of the deep bulk. From figures 1 and 2, the boundary-layer thickness is about $0.05h$, hence the diffusive equilibration of the boundary layer occurs on a tiny fraction $(1/400)$ of the vertical diffusive timescale h^2/κ.

Numerical resolution of the small spatial scales and fast velocities characteristic of the initial transient in figure 4 makes strong demands on both spatial resolution and time-stepping. To reduce the strength of this transient, particularly for 3D integrations with Ra greater than about 10^9, we experimented with buoyancy initial condition such as $b(x, y, z, 0) = -0.74 b_\star$. This "cold start" ensures that the flow begins closer to its ultimate sluggish state, thus rendering the initial transient much less energetic. The cold start makes far less arduous computational demands, both because the weaker transient requires less spatial and temporal resolution and because the $Nu(t)$ equilibrates even faster than in figure 4: see figure 5.

In figure 5 we used the cold initial buoyancy $-0.74 b_\star$ that is suggested by the long calculation in figure 4(c). But usually one must guess at the initial buoyancy which is closest to the ultimate bottom buoyancy. The three solutions shown in figure 6 indicate that the consequences of a guess that is too cold are not serious. The solution with initial

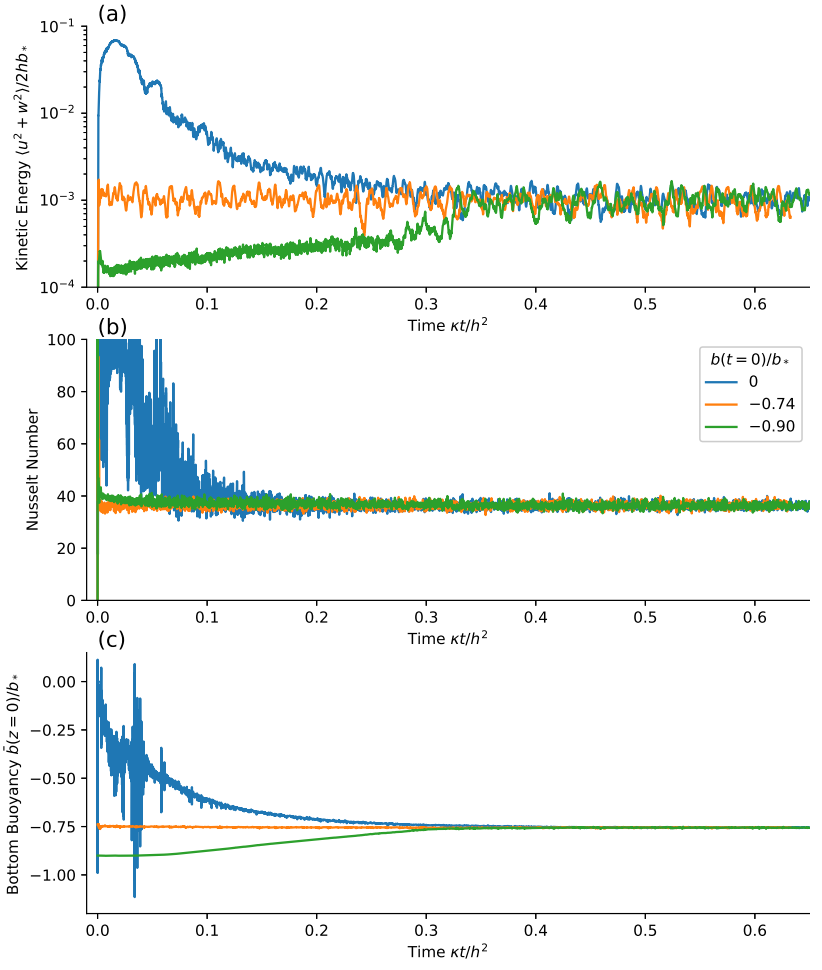

FIGURE 6. Approach to statistical equilibrium for 2D free-slip simulations at $Ra = 6.4 \times 10^{10}$. We show three initial buoyancy conditions $b(x, z, 0) = b_\star \times (0, -0.74, -0.9)$. (a) Domain-averaged kinetic energy. (b) The Nusselt number $Nu(t)$. (c) The bottom buoyancy $\bar{b}(z = 0)/b_\star$.

buoyancy $b(x, z, 0) = -0.9b_\star$ is too cold: the bottom buoyancy must increase to about $-0.75b_\star$ in the long-time state. Nonetheless, the Nusselt number of the too-cold solution in figure 6(b) equilibrates quickly. Moreover to estimate Nu it is better to start too cold than too warm: the too-warm initial condition in figure 6, i.e., $b(x, z, 0) = 0$, has a large initial transient in the kinetic energy and $Nu(t)$ does not stabilize till about $t = 0.2h^2/\kappa$. The kinetic energy and bottom buoyancy in figure 6(a) and (c) require longer evolution than $Nu(t)$ in order to achieve their final values.

To conclude this section, we note that the identity (3.7) provides an alternative means of diagnosing the Nu by measuring the buoyancy flux $\kappa b_z(x, y, h, t)$ through the top surface of the domain. We refer to this second Nusselt number as the "surface Nusselt number", denoted $Nu_{\rm s}(t)$. Multiplying the buoyancy equation (2.2) by b, and integrating over the volume of the domain, we obtain

$$\frac{\mathrm{d}}{\mathrm{d}t}\int \tfrac{1}{2}b^2\,\mathrm{d}V = \int_{z=h} b_{\rm s}\,\kappa b_z\,\mathrm{d}A - \kappa\int |\boldsymbol{\nabla} b|^2\,\mathrm{d}V\,. \tag{4.3}$$

This shows that the difference between $Nu_{\rm s}(t)$ and $Nu(t)$ — the two terms on the right

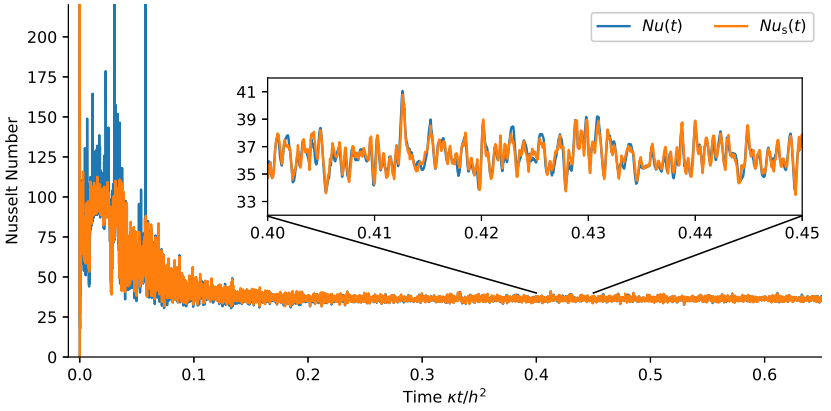

FIGURE 7. A comparison of the "instantaneous Nusselt number" time-series for the 2D free-slip solution at $Ra = 6.4 \times 10^{10}$ with initial condition $b(x, z, 0) = 0$. $Nu(t)$ is defined via the volume average of $\kappa|\boldsymbol{\nabla} b|^2$, i.e., the second term on the right of (4.3). The surface Nusselt number, $Nu_s(t)$, is defined via the surface average of b_s times the flux $\kappa b_z(x, h, t)$, i.e., the first term on the right of (4.3).

of (4.3) — is related to temporal fluctuations in the domain integrated buoyancy variance. The buoyancy power integral (3.7) is obtained by time-averaging (4.3).

Figure 7 shows that during the initial transient there are substantial differences between $Nu(t)$ and $Nu_s(t)$. But after about $t = 0.15h^2/\kappa$, $Nu(t)$ and $Nu_s(t)$ almost coincide. This coincidence indicates that in the final statistically steady state the left hand side of (4.3) is a small residual between the two much larger terms on the right. This is another indication that the buoyancy boundary layer is strongly controlled by diffusion.

Direct evaluation of χ via definition (3.5) requires the volume integral of the squared buoyancy gradient, which is concentrated on small spatial scales. In an experimental situation this is likely impossible. The identity (4.3) shows that χ can alternatively be estimated from a surface integral involving the vertical buoyancy flux through the nonuniform surface. Figure 3(a) indicates that the surface flux is a large-scale quantity. Thus Nu_s is more accessible to experimental measurement.

5. Conclusion

We advocate adoption of the χ-based Nusselt number in (3.6) as the primary index of the strength of HC. The identity

$$\overline{\boldsymbol{J} \cdot \boldsymbol{\nabla} b_s} = -\chi \,. \tag{5.1}$$

provides a connection between this Nu and the horizontal buoyancy flux $\boldsymbol{J}$. Using (5.1) one can introduce the effective diffusivity D in (3.15) and (3.16); figure 3(b) shows that D provides a good diagnostic of the relation between the surface buoyancy gradient $\boldsymbol{\nabla} b_s$ and $\boldsymbol{J}$. In section 4 we showed that $Nu(t)$ equilibrates more rapidly than other average properties of HC, such as volume-averaged kinetic energy and bottom buoyancy. With a "cold start" the long-term average of $Nu(t)$ can be estimated with integrations that are much shorter than a diffusive time scale: see figures 5 and 6(b). These numerical results indicate that buoyancy variance dissipation on the right of (5.1) is strongly concentrated in an upper boundary layer and that fast diffusion through this thin layer results in relatively rapid equilibration of Nu.

The definition of Nu in (3.6) also applies to Rayleigh-Bénard convection. Thus the

diffusive dissipation of buoyancy variance on the right of (5.1) emerges as the prime index of the strength of both varieties of convection.

The authors report no conflict of interest. We thank Taimoor Sohail for help with figure 1 and Basile Gallet and Thomas Bossy for discussion of horizontal convection. Computer resources were provided by the Australian National Computational Infrastructure at ANU, which is supported by the Commonwealth of Australia. WRY was supported by the National Science Foundation Award OCE-1657041.

REFERENCES

Burns, K. J., Vasil, G. M., Oishi, J. S., Lecoanet, D. & Brown, B. P. 2019 Dedalus: A flexible framework for numerical simulations with spectral methods. *Physical Review Research* (accepted, arXiv:1905.10388).

Doering, C. R. & Constantin, P. 1996 Variational bounds on energy dissipation in incompressible flows. III. Convection. *Physical Review E* **53** (6), 5957.

Gayen, B., Griffiths, R. W. & Hughes, G. O. 2014 Stability transitions and turbulence in horizontal convection. *Journal of Fluid Mechanics* **751**, 698–724.

Gayen, B., Griffiths, R. W., Hughes, G. O. & Saenz, J. A. 2013 Energetics of horizontal convection. *Journal of Fluid Mechanics* **716**, R10.

Griffiths, R. W., Hughes, G. O. & Gayen, B. 2013 Horizontal convection dynamics: insights from transient adjustment. *Journal of Fluid Mechanics* **726**, 559–595.

Howard, L. N. 1963 Heat transport by turbulent convection. *Journal of Fluid Mechanics* **17** (3), 405–432.

Hughes, G. O. & Griffiths, R. W. 2008 Horizontal convection. *Annu. Rev. Fluid Mech.* **40**, 185–208.

Ilicak, M. & Vallis, G. K. 2012 Simulations and scaling of horizontal convection. *Tellus A: Dynamic Meteorology and Oceanography* **64** (1), 18377.

Mullarney, J. C., Griffiths, R. W. & Hughes, G. O. 2004 Convection driven by differential heating at a horizontal boundary. *Journal of Fluid Mechanics* **516**, 181–209.

Paparella, F. & Young, W. R. 2002 Horizontal convection is non-turbulent. *Journal of Fluid Mechanics* **466**, 205–214.

Passaggia, P.-Y., Scotti, A. & White, B. 2017 Transition and turbulence in horizontal convection: linear stability analysis. *Journal of Fluid Mechanics* **821**, 31–58.

Rocha, C.B., Bossy, T., Llewellyn Smith, S.G. & Young, W. R. 2020 Improved bounds on horizontal convection. *Journal of Fluid Mechanics* **883**, A41.

Rosevear, M. G., Gayen, B. & Griffiths, R. W. 2017 Turbulent horizontal convection under spatially periodic forcing: a regime governed by interior inertia. *Journal of Fluid Mechanics* **831**, 491–523.

Rossby, H. T. 1965 On thermal convection driven by non-uniform heating from below: an experimental study. *Deep Sea Research and Oceanographic Abstracts* **12** (1), 9–10, IN9–IN14, 11–16.

Rossby, H. T. 1998 Numerical experiments with a fluid heated non-uniformly from below. *Tellus A* **50** (2), 242–257.

Scotti, A. & White, B. 2011 Is horizontal convection really "non-turbulent?". *Geophysical Research Letters* **38** (21), L21609.

Sheard, G. J. & King, M. P. 2011 Horizontal convection: effect of aspect ratio on Rayleigh number scaling and stability. *Applied Mathematical Modelling* **35** (4), 1647–1655.

Shishkina, O., Grossmann, S. & Lohse, D. 2016 Heat and momentum transport scalings in horizontal convection. *Geophysical Research Letters* **43** (3), 1219–1225.

Siggers, J. H., Kerswell, R. R. & Balmforth, N. J. 2004 Bounds on horizontal convection. *Journal of Fluid Mechanics* **517**, 55–70.

Wang, W. & Huang, R. X. 2005 An experimental study on thermal convection driven by horizontal differential heating. *Journal of Fluid Mechanics* **540**, 49–73.

Winters, K. B. & Young, W. R. 2009 Available potential energy and buoyancy variance in horizontal convection. *Journal of Fluid Mechanics* **629**, 221–230.